

Five Planets and an Independent Confirmation of HD 196885Ab from Lick Observatory ¹

Debra Fischer^{2,3}, Peter Driscoll⁴, Howard Isaacson², Matt Giguere^{2,3}, Geoffrey W. Marcy⁵,
Jeff Valenti⁶, Jason T. Wright⁷, Gregory W. Henry⁸, John Asher Johnson⁹, Andrew
Howard⁵, Katherine Peek⁵, Chris McCarthy²

fischer@stars.sfsu.edu

ABSTRACT

We present time series Doppler data from Lick Observatory that reveal the presence of long-period planetary companions orbiting nearby stars. The typical eccentricity of these massive planets are greater than the mean eccentricity of known exoplanets. HD 30562b has $M \sin i = 1.29 M_{\text{Jup}}$, with semi-major axis of 2.3 AU and eccentricity 0.76. The host star has a spectral type F8V and is metal rich. HD 86264b has $M \sin i = 7.0 M_{\text{Jup}}$, $a_{\text{rel}} = 2.86$ AU, an eccentricity, $e = 0.7$ and orbits a metal-rich, F7V star. HD 87883b has $M \sin i = 1.78 M_{\text{Jup}}$, $a_{\text{rel}} = 3.6$ AU, $e = 0.53$ and orbits a metal-rich K0V star. HD89307b has $M \sin i = 1.78 M_{\text{Jup}}$, $a_{\text{rel}} = 3.3$ AU, $e = 0.24$ and orbits a G0V star with slightly subsolar metallicity. HD 148427b has $M \sin i = 0.96 M_{\text{Jup}}$, $a_{\text{rel}} = 0.93$ AU, eccentricity of

¹Based on observations obtained at the Lick Observatory, which is operated by the University of California

²Department of Physics & Astronomy, San Francisco State University, San Francisco, CA 94132

³Department of Astronomy, Yale University, New Haven, CT 06511

⁴Department of Earth and Planetary Science, Johns Hopkins University, Baltimore, MD

⁵Department of Astronomy, University of California, Berkeley, Berkeley, CA

⁶Space Telescope Science Institute, Baltimore, MD

⁷Cornell University, Ithaca, NY

⁸Center of Excellence in Information Systems, Tennessee State University, 3500 John A. Merritt Blvd., Box 9501, Nashville, TN 37209

⁹NSF Astronomy & Astrophysics Postdoctoral Fellow, Institute for Astronomy, University of Hawaii, Honolulu, HI 96822

0.16 and orbits a metal rich K0 subgiant. We also present velocities for a planet orbiting the F8V metal-rich binary star, HD 196885A. The planet has $M \sin i = 2.58 M_{\text{Jup}}$, $a_{\text{rel}} = 2.37$ AU, and orbital eccentricity of 0.48, in agreement with the independent discovery by Correia et al. (2008).

Subject headings: planetary systems – stars: individual (HD 30562, HD 86264, HD 87883, HD 89307, HD 148427, HD 196885)

1. Introduction

Over the past 14 years, more than 300 extrasolar planets have been discovered orbiting sunlike stars. Most of these discoveries were made with high precision Doppler observations that measure the reflex radial velocity of the host star. Radial velocity amplitudes scale with the mass of the planet and are inversely proportional to the cube root of the orbital period. Therefore, detectability in Doppler surveys is enhanced for short period orbits and massive exoplanets. An additional constraint on detectability is that at least one full orbital period must be observed in order to accurately model the Doppler velocity data with a Keplerian orbit. As a result, about 85% of detected exoplanets have $M \sin i$ greater than the mass of Saturn; most have orbital periods shorter than four years (e.g., see <http://exoplanets.eu>) Higher cadence observations and improved Doppler precision are now enabling the detection of both lower mass (Bouchy et al. 2009; Mayor et al. 2009a,b; Howard et al. 2009) and longer period (Moutou et al. 2009) exoplanets.

The planet survey at Lick Observatory began in 1989 and is one of the oldest continuous Doppler programs in the world (Marcy et al. 1997). Because of this long time baseline of data, 55 Cnc d, the only planet with complete phase coverage and a well determined orbital period greater than ten years was discovered at Lick Observatory (Marcy et al. 2002). The original Lick program contained ~ 100 stars. In 1997, the sample was augmented to ~ 400 stars (Fischer et al. 1999). In this paper, we describe the detection of single planets orbiting HD 30562, HD 86264, HD 89307, HD 87883, HD 148427, and HD 196885Ab that have emerged from that extended sample. All are fairly massive planets ($M \sin i > 0.96 M_{\text{Jup}}$) in relatively long period ($P > 333$ d) orbits that exhibit significant orbital eccentricities.

2. Doppler Analysis

Our Doppler analysis makes use of an iodine absorption cell in the light path before the entrance slit of the spectrometer. The iodine absorption lines in each program observation

are used to model the wavelength scale and the instrumental profile of the telescope and spectrometer optics for each observation (Marcy & Butler 1992; Butler et al. 1996) The iodine cell at Lick Observatory has not been changed over the entire duration of the planet search project, helping to preserve continuity in our velocity measurements despite three CCD detector upgrades. The velocity precision for the Lick project is generally photon-limited with typical signal-to-noise ~ 120 . To improve the precision, consecutive observations are sometimes independently analyzed and a single weighted mean velocity is determined.

In addition to photon statistics, there are sources of systematic errors. For example, the Hamilton spectrometer (Vogt et al. 1987) resides in the Coudé room and is not temperature controlled. Diurnal temperature variations of several degrees can occur in addition to seasonal temperature swings of about ~ 25 C. Temperature and pressure changes can lead to gradual changes in the PSF through the night. Even more rapid PSF variations occur as guiding errors or changes in seeing shift the spectrum by a few tenths of a pixel (i.e., ~ 400 m s $^{-1}$) on the CCD. Ultimately, the burden for tracking all of these systematic sources of error is placed on our ability to model the PSF from the iodine absorption lines in each program observation.

Because the PSF varies over the detector, the Doppler analysis is carried out independently in wavelength chunks that span about 3\AA of the spectrum. In each of these chunks, we model the wavelength solution, the PSF and the Doppler shift of the star. Each chunk is compared differentially to chunks from previous observations containing the same spectral lines. The median velocity for all the chunks yields the differential velocity measurement. The standard deviation of the velocities from the several hundred chunks provides an assessment of the uncertainty in the velocity measurement, but can be an underestimate of the residual RMS scatter arising from instrumental sources or additional unidentified planets.

2.1. Jitter

The Doppler analysis provides formal measurement errors, however additional systematic noise in the center of mass velocity of the star can arise and are more difficult to characterize. The systematic errors can either be intrinsic to velocity fields in the stellar atmospheres, or, as described in the previous section, they can be the result of instrumental effects that are inadequately modeled in our Doppler analysis. Unfortunately, it is often difficult to identify the source of spurious velocity variations. For example, Queloz et al. (2001) measured velocity variations in HD 165435 with an amplitude of 80 m s $^{-1}$ that correlated with photometric variability. However, systematic studies of activity and velocity variations (Saar, Butler, Marcy 1998; Saar & Fischer 1999) have shown that it is difficult to identify

unambiguous correlations between astrophysical parameters and velocity variations.

Isaacson & Fischer (2009) have measured emission in the Ca II H & K line to produce S_{HK} values that are calibrated to the canonical Mt Wilson values (Duncan et al. 1991) following Wright (2005). The S_{HK} values are used to calculate $\log R'_{\text{HK}}$, the ratio of emission in the cores of the Ca II H & K lines to the flux in the photosphere, and to estimate rotational periods (Noyes et al. 1984). They searched for correlations between $\log R'_{\text{HK}}$ values and radial velocity “jitter” using the highest precision velocity data sets from the California Planet Search survey, obtained after the CCD upgrade (August 2004) at Keck Observatory. Their model of jitter has a functional dependence on (1) $\log R'_{\text{HK}}$, (2) height above the main sequence (evolutionary status), and (3) $B-V$ color. We adopt their model as an independent estimate of jitter (which likely includes some systematic instrumental errors in addition to astrophysical noise) that is added in quadrature to formal velocity errors when fitting Keplerian models to the data. These augmented errors are included in the calculation of χ^2_ν and in the Figures showing Keplerian fits to the data; however, they are not included in the tabulated velocity errors for the time series data. To reproduce the errors used in Keplerian fitting, the stellar jitter values should be added in quadrature to errors reported in the individual radial velocity Tables.

3. Keplerian Fitting

3.1. Levenberg Marquardt Fitting

Time series velocity data are fit with a Keplerian model using the partially linearized Levenberg-Marquardt minimization algorithm described in Wright & Howard (2009). The Levenberg-Marquardt algorithm employs a gradient search to minimize the χ^2_ν fit between an assumed Keplerian model and the observed data. The free parameters for each planet in the Keplerian model include the orbital period, P , the time of periastron passage, T_P , the orbital eccentricity, e , the argument of periastron passage referenced to the ascending node, ω and the velocity semi-amplitude, K . The velocity for the center of mass, γ , is an additional single free parameter for a system of one or more planets. The Keplerian model with the minimum χ^2_ν value provides the maximum likelihood estimate for the orbital parameters. While this approach is quite efficient for well-sampled data sets, it is possible for the fitting algorithm to become trapped in a local χ^2_ν minimum. Particularly when there are unobserved gaps in the orbital phase, covariance between the orbital parameters can be significant and Keplerian fitting with a Levenberg-Marquardt algorithm does not capture the full range of possible orbital parameters.

Typically, $N = 1000$ Monte Carlo trials are run with Levenberg-Marquardt Monte Carlo (LMMC) fitting, scrambling the residuals (with replacement of previously selected values) before adding the theoretical velocities back in and refitting new Keplerian models using the Levenberg-Marquardt algorithm. For Gaussian velocity errors, mean values from the Monte Carlo trials define the parameter value. The standard deviation of the trial parameters defines the uncertainties.

3.2. Markov Chain Monte Carlo Fitting

Following a technique outlined by Ford (2005) we have also tested a Markov Chain Monte Carlo (MCMC) algorithm to derive Keplerian fits and to characterize uncertainties in the orbital parameters (Driscoll, Fischer, & Ford 2009). The MCMC algorithm is a Bayesian technique which samples the orbital parameters in proportion to an expected posterior probability distribution. It allows for larger steps in parameter space than a routine driven only by χ^2_ν minimization, enabling a more complete exploration of parameter space.

One drawback of the MCMC method is that, since each step in the Markov chain is correlated with the previous step, MCMC can give misleading results if the Markov chain has not converged. For systems that do converge, the MCMC method provides a more robust characterization of the uncertainties in orbital parameters, particularly when the observational data results in either a rough χ^2_ν surface or a χ^2_ν surface with a shallow minimum. For data sets where the observations span multiple orbital periods with complete phase coverage, the MCMC algorithms converge to the same solutions obtained by the frequentist Levenberg-Marquardt algorithm (Driscoll, Fischer, & Ford 2009).

4. HD 30562

4.1. Stellar Characteristics

HD 30562 (HIP 22336, $V = 5.77$, $B - V = 0.63$) is a F8V star. The Hipparcos parallax (ESA 1997) yields a distance of 26.5 pc. Isaacson & Fischer (2009) find that HD 30562 is chromospherically inactive and measure $S_{\text{HK}} = 0.15$, $\log R'_{\text{HK}} = -5.064$. Based on their model of stellar jitter, we estimate a jitter of 2.9 m s^{-1} for this star. We estimate a rotational period, $P_{\text{rot}} = 24.2 \text{ d}$, using the calibration by Noyes et al. (1984).

A high resolution spectroscopic analysis has been carried out for all of the stars in this paper, including HD 30562, using spectroscopic modeling with SME (Valenti & Piskunov

1996). The analysis that was reported in Valenti & Fischer (2005) has been further refined, following the method described in Valenti et. al. (2009): the SME spectroscopic solution for surface gravity is determined iteratively with interpolation of the Yonsei-Yale (“Y2”) isochrones (Demarque et al. 2004). This analysis yields $T_{\text{eff}} = 5861 \pm 44\text{K}$, $\log g = 4.088 \pm 0.06$, $v \sin i = 4.9 \pm 0.50 \text{ km s}^{-1}$, $[\text{Fe}/\text{H}] = 0.243 \pm 0.04 \text{ dex}$. The isochrone analysis yields the same value for surface gravity (by design) and a stellar luminosity of $L_{\star} = 2.85L_{\odot}$ with a bolometric correction of $\text{BC} = -0.064$, a stellar mass of $1.219M_{\odot}$ and a stellar radius of $1.637 R_{\odot}$. This compares well with the stellar mass and luminosity derived by Takeda et al. (2007) who model stellar evolution tracks using the spectroscopic model parameters. The stellar parameters described here are summarized in Table 1.

4.2. Doppler Observations and Keplerian Fit

We have acquired 45 Doppler measurements of HD 30562 over the past ten years. With typical seeing at Lick of $1''.5$, the exposure time for SNR of 140 is about 5 minutes on the 3-m Shane telescope or about 30 minutes on the 0.6-m Coudé Auxiliary Telescope (CAT).

The observation dates, radial velocities and measurement uncertainties are listed in Table 2. The initial phase coverage was rather poor, however, after velocity variations were detected we redoubled our efforts and obtained additional (co-added) observations using the 0.6-m CAT to fill in phase coverage since 2006. The best fit LMMC Keplerian model has a period of $P = 1157 \pm 27 \text{ days}$, a semi-velocity amplitude $K = 33.7 \pm 2.2 \text{ m s}^{-1}$ and orbital eccentricity, $e = 0.76 \pm 0.05$. The mean RMS to the fit is 7.58 m s^{-1} . Including the estimated jitter of 2.9 m s^{-1} we obtain $\chi_{\nu}^2 = 1.31$ as a measure of the goodness of the model fit. Adopting a stellar mass of $1.219 M_{\odot}$, we derive $M \sin i = 1.29 M_{\text{Jup}}$ and a semi-major axis of 2.3 AU.

As described above, uncertainties in the orbital parameters were determined by running 1000 LMMC trials. In each trial, the theoretical fit was subtracted from radial velocities and the residual velocities were scrambled and added back to the theoretical velocities. A new trial Keplerian fit was then obtained. The standard deviation of each orbital parameter for the 1000 Monte Carlo trials was adopted as the parameter uncertainty. The Keplerian orbital solution is listed in Table 3 and the time series velocity data are plotted with the best-fit Keplerian model (solid line) in Figure 1.

We also carried out an MCMC fit for HD 30562. The radial velocity data have good phase coverage for this system, and so the agreement between the LMMC and MCMC fits are quite good. The modest covariance between the velocity amplitude and orbital eccentricity

is shown in Figure 2, however, the best χ^2_ν contours are consistent with the formal parameter errors derived from the LMMC analysis.

5. 86264

5.1. Stellar Characteristics

HD 86264 (HIP 48780) is an F7V star with apparent brightness, $V = 7.42$, and color $B - V = 0.46$. Based on the parallax measurement from Hipparcos (ESA 1997) of 13.78 mas , this star is located at a distance of about 72 parsec with an absolute visual magnitude of $M_V = 3.10$. Using spectral synthesis modeling and iterating until there is a match in surface gravity with the value predicted from interpolation of the Y2 isochrones, we derive $T_{\text{eff}} = 6210 \pm 44\text{K}$, $\log g = 4.02$, $v \sin i = 12.8 \text{ km s}^{-1}$, $[\text{Fe}/\text{H}] = +0.202$. The bolometric correction is -0.024 , stellar luminosity is $L_\star = 4.55 L_\odot$, $R_\star = 1.88 R_\odot$, and $M_\star = 1.42 M_\odot$. The star is moderately active, with $S_{\text{HK}} = 0.20$ and $\log R'_{\text{HK}} = -4.73$. The expected jitter from Isaacson & Fischer (2009) is 3.3 m s^{-1} . The stellar characteristics are compiled in Table 1.

5.2. Doppler Observations and Keplerian Fit

HD 86264 has been on the Lick program since January 2001 and exhibits a large amplitude velocity variation with a periodicity of about 4 years. The expected jitter for this star is likely higher than predicted because the star is a relatively rapid rotator. For this reason, and because the star is at the faint magnitude limit of our program, we typically limited our exposure time and obtained SNR of only 80 to 100. Our mean velocity precision for HD 86264 is 21 m s^{-1} (probably set both by the relatively low SNR for our observations and the relatively high vsini of the star). As a result, only planets with relatively large velocity amplitudes would have been detected around this star.

A total of 37 radial velocity measurements are listed in Table 4. A periodogram of the velocities shows a strong broad peak at about 1475 days with an FAP less than 0.0001 or 0.01%. The Keplerian model was derived with a Levenberg-Marquardt (LMMC) fitting algorithm with an assumed stellar jitter of 3.3 m s^{-1} added in quadrature to the formal velocity errors. The best fit LMMC solution has a period of $P = 1475 \pm 55\text{d}$, velocity amplitude, $K = 132 \text{ m s}^{-1}$, and eccentricity $e = 0.7$. However, the LMMC trials revealed an asymmetry in the distribution of modeled velocity amplitudes. While K was rarely less than 120 m s^{-1} , some models were found with K up to 246 m s^{-1} . Furthermore, a large

standard deviation in the 1000 trials was found for the orbital eccentricity. The χ^2_ν fits for eccentricities down to 0.4 were only worse by 5%, with $\chi^2_\nu = 1.28$.

The linear trend included in the LMMC Keplerian model has a positive slope of about 1.8 m s^{-1} per year or 16.4 m s^{-1} over the nine year duration of velocity measurements. This slope is only marginally significant given the large uncertainty in the radial velocity measurements for this star, however it was retained because of the significant improvement to χ^2_ν . We note that a similar improvement in χ^2_ν could have been achieved by adopting a larger (and still physically plausible) value for jitter.

The implied planet mass is $M \sin i = 7 M_{\text{Jup}}$ with a semi-major axis of 2.86 AU. The LMMC Keplerian solution is summarized in Table 3. The time series velocity measurements are plotted in Figure 3. The LMMC Keplerian model with best fit eccentricity of 0.7 is indicated in Figure 3 with a solid line and a Keplerian model with eccentricity of 0.4 is overplotted with a dashed line. Although the difference between 0.4 and 0.7 is substantial, it is apparent from Figure 3 that the solutions are nearly consistent with either value, resulting in a modest 5% penalty in χ^2_ν .

The radial velocity data set for HD 86264 has a gap in the time series data as the planet approaches periastron. As a result, the LMMC fitting algorithm may not have captured the full range of possible parameters (also suggested by the large uncertainty in eccentricity and velocity amplitude). The probability density functions from the MCMC simulations are plotted in Figure 4 and show general agreement with the LMMC trials. However, the MCMC simulations quantify a broader range of parameter values, particularly for orbital eccentricity and the velocity amplitude. The covariance of these two parameters is illustrated in Figure 5; eccentricity is correlated with velocity amplitude because of the gap in the time-series velocity measurements.

5.3. Photometry

HD 86264 is the only star in the present sample for which we have photometric observations. The star was observed in the Johnson B and V pass bands by the T3 0.4 m automatic photometric telescope (APT) at Fairborn Observatory as one of two comparison stars for another observing program (Henry, Fekel, & Henry 2007, Tables 3 and 4). Details of the T3 APT, the differential observing sequence, and the reduction of the data are given in that same paper.

Between 2003 November and 2004 May, the T3 APT acquired 239 good observations in the V band and 232 observations in B . We have reanalyzed these observations from

Henry, Fekel, & Henry (2007) for the present study, searching for low-amplitude variability that might allow the direct determination of the star’s rotation period. With a log R’HK value of -4.73, HD 86264 is the most active star in our sample and so a good candidate for exhibiting starspot activity, which might result in detectable rotational modulation of the star’s brightness (Henry 1999, see Figure 11).

The *Hipparcos* catalog (ESA 1997) lists 107 photometric measurements acquired during the mission between 1989 November and 1993 March, but the *Hipparcos* team does not venture a variability classification. Our 2003–04 APT measurements have standard deviations of 0.0065 and 0.0064 in the B and V , respectively. These values agree with typical scatter observed in constant stars measured with the T3 APT. Power spectrum analysis fails to find any significant periodicity between one and 25 days and limits the semi-amplitude of any real signal within this period range to a maximum of ~ 0.0015 mag.

We were somewhat surprised by our failure to detect rotational variability in HD 86264, given its modest activity level. However, we note from Tables 1 and 8 that HD 86264 has the lowest color index in the sample ($B - V = 0.46$) and thus a relatively shallow convection zone. Furthermore, the *estimated* rotation period, stellar radius, and observed $v \sin i$ given in Table 1 imply a low equatorial inclination of $\sim 30^\circ$. Both of these factors work to minimize observable rotational variability in HD 86264. Surface magnetic activity should not have a significant effect on the measured radial velocities.

6. 87883

6.1. Stellar Characteristics

HD 87883 (HIP 49699) is a K0V star with $B - V = 0.96$ and Hipparcos parallax based distance of 18 parsecs. The star has a V magnitude of 7.57 and an absolute visual magnitude, $M_V = 6.3$. Isaacson & Fischer (2009) measure modest chromospheric activity with an S_{HK} value of 0.26, $\log R'_{\text{HK}} = -4.86$ and predict a stellar jitter of 4.5 m s^{-1} . The rotation period predicted from this activity level is 41.2 days (Noyes et al. 1984). We again adopt an iterative approach to tie surface gravity from the spectroscopic analysis to the Y2 isochrone interpolation. The surface gravity converges at $\log g = 4.58$ and yields $T_{\text{eff}} = 4980 \pm 44 \text{ K}$, $[\text{Fe}/\text{H}] = +0.093$, $v \sin i = 2.2 \text{ km s}^{-1}$ in good agreement with the original analysis of Valenti & Fischer (2005). The stellar luminosity is $L_\star = 0.318 L_\odot$, stellar radius is $R_\star = 0.76 R_\odot$, and stellar mass is $0.82 M_\odot$. The stellar parameters are summarized in Table 1.

6.2. Doppler Observations and Keplerian Fit

HD 87883 has been observed at Lick Observatory since December 1998. The 44 radial velocity measurements from Lick Observatory are listed in Table 5, along with the observation dates and uncertainties. The mean signal-to-noise of 120 for the observations produces a typical velocity measurement uncertainty of 4 m s^{-1} . The data were initially fit with a single planet model with a period of 7.9 years. The initial rms of the Keplerian fit was surprisingly high, 9.0 m s^{-1} . After adding the expected jitter of 4.5 m s^{-1} in quadrature with the internal errors, we found a relatively poor χ^2_ν of 1.7, suggesting that the single planet model was not adequate. The velocity residuals to the prospective Keplerian model of the Lick data showed only a modest peak in the periodogram.

In an effort to better understand the residual velocities, we obtained 25 additional velocity measurements from the Keck Observatory. These velocities are included in Table 5 with a designation of “K” in the “Observatory” column to distinguish them from the Lick observations. The average signal-to-noise at Keck is 220 and the single measurement precision is $\sim 2.2 \text{ m s}^{-1}$, providing higher quality velocity measurements. The Lick and Keck velocities were merged with velocity offset as a free parameter to minimize χ^2_ν of the Keplerian fit. The velocity offset was only 1.6 m s^{-1} for these two data sets and has been subtracted from the Keck radial velocity measurements listed in Table 5.

The combined Lick and Keck velocities were modeled with a Keplerian with a period of 7.9 years, an eccentricity of $e = 0.53$, and velocity semi-amplitude of $K = 34.7 \text{ m s}^{-1}$. The velocities are plotted in Figure 6 with the expected 4.5 m s^{-1} jitter added in quadrature with the formal errors. After fitting the combined Lick and Keck velocities, the rms for the Keck data alone was 8.6 m s^{-1} and the rms for the combined data sets was 9.2 m s^{-1} with a $\chi^2_\nu = 1.71$. The periodogram of the residuals to the fit (with combined Lick and Keck data) does not show any significant power. Continued observations may eventually reveal an additional short-period planetary companion. Alternatively, a background star, blended with the image of HD 87883 on the slit could also introduce unexpected velocity variations. Since the star is relatively close (18 parsecs) a stellar companion separated by less than $0''.5$ might be resolvable with adaptive optics observations and would be helpful for understanding the high rms to our Keplerian fit.

7. 89307

7.1. Stellar Characteristics

HD 89307 (HIP 50473) is a G0V star with an apparent magnitude of $V = 7.06$ and $B - V = 0.640$. The Hipparcos-based distance is 30.9 parsecs implying an absolute visual magnitude of $M_V = 4.57$. Our spectroscopic analysis yields $T_{\text{eff}} = 5950 \pm 44\text{K}$, $\log g = 4.414 \pm 0.10$, $v \sin i = 3.21 \pm 0.50 \text{ km s}^{-1}$, $[\text{Fe}/\text{H}] = -0.14 \pm 0.04$ dex. The $\log g$ value in the spectroscopic model was tied to the Y2 isochrones, which yield a stellar luminosity of $1.24 L_{\odot}$ with a bolometric correction of -0.075 , radius of $1.05 R_{\odot}$ and stellar mass of $1.028 M_{\odot}$, in good agreement with Takeda et al. (2007) who derive a stellar mass of $0.989 M_{\odot}$, age of 6.76 Gyr, a stellar radius of $1.1 R_{\odot}$ and $\log g$ of 4.36.

HD 89307 is chromospherically inactive with a measured $S_{\text{HK}} = 0.154$, $\log R'_{\text{HK}} = -4.98$, and estimated velocity jitter of 2.8 m s^{-1} . The inferred rotational period from the chromospheric activity is 23.7d. The stellar properties of HD 89307 are compiled in Table 1.

7.2. Doppler Observations and Keplerian Fit

We obtained 59 observations of HD 89307 with a typical SNR of 120 using the Shane 3m telescope at Lick Observatory over the past ten years, yielding a mean velocity precision of about 6 m s^{-1} . The orbital solution was presented before the orbital solution was secure in Fischer & Valenti (2005) with an orbital period of 3090 days and in Butler et al. (2006) with an orbital period of 2900 ± 1100 d ays.

The observation dates, radial velocities and instrumental uncertainties for this system are listed in Table 6. The time series data are plotted in Figure 8 and exceed more than one full orbit. The data were fit with a Keplerian model using a Levenberg-Marquardt algorithm (LMMC). The best fit orbital solution has a period, $P = 2157 \pm 63$ d; eccentricity, $e = 0.241 \pm 0.07$; and velocity semi-amplitude, $K = 28.9 \pm 2.2 \text{ m s}^{-1}$. With the assumed stellar mass of $1.028 M_{\odot}$ for this slightly metal-poor star, we derive a planet mass, $M \sin i = 1.78 M_{\text{Jup}}$ and semi-major axis of 3.27 AU. The χ^2_{ν} for this fit is 1.37 with an RMS of 9.9 m s^{-1} . Orbital parameters for HD 89307 are listed in Table 3.

8. HD 148427

8.1. Stellar Characteristics

HD 148427 (HIP 80687) is a moderately evolved K0 subgiant with an apparent brightness $V = 6.9$ and $B - V$ color 0.98. A distance of 59.3 parsec was derived from the Hipparcos parallax of 16.87 mas , which yields an absolute magnitude $M_V = 3.02$ and luminosity of $6 L_\odot$ for this star. Spectroscopic modeling of the star provides $T_{\text{eff}} = 5052 \pm 44\text{K}$, $\log g = 3.586 \pm 0.10$, $v \sin i = 2.13 \text{ km s}^{-1}$ and $[\text{Fe}/\text{H}] = 0.154 \pm 0.04$. Our iterative interpolation of the Y2 isochrones yields a stellar mass of $1.45 M_\odot$, stellar radius of $3.22 R_\odot$ in good agreement with Takeda et al. (2007) who also derive an age of 2.5 Gyr from evolutionary tracks. Isaacson & Fischer (2009) derive $S_{\text{HK}} = 0.14$, $\log R'_{\text{HK}} = -5.18$ and a stellar jitter of 3.5 m s^{-1} . The stellar parameters are summarized in Table 1.

8.2. Doppler Observations and Keplerian Fit

HD 148427 has been observed at Lick since 2001 with a typical SNR of 120 and single measurement uncertainties of about 4 m s^{-1} . The radial velocity observations of this star are listed in Table 7. The periodogram of these velocities has a strong peak at about 331 days with an FAP less than 0.01%. The data are well-modeled with a Keplerian orbit that has a period of 331.5 ± 3.0 days, velocity semi-amplitude of $27.7 \pm 2 \text{ m s}^{-1}$, and an eccentricity of 0.16 ± 0.08 . Adopting the stellar mass of $1.45 M_\odot$, we derive a planet mass, $M \sin i = 0.93 M_{\text{Jup}}$ and an earthlike orbital radius of 0.96 AU. The orbital solution is listed in Table 3. The radial velocity measurements are plotted with jitter of 3.5 m s^{-1} added in quadrature in Figure 9 to yield a χ^2_ν fit of 1.08 with an rms of 7.0 m s^{-1} . The phase-folded Keplerian model is overplotted in Figure 9 as a dashed line.

9. HD 196885 A

We began observing HD 196885 A at Lick Observatory in 1998. In 2004 the velocity variations for this star were modeled with a preliminary orbital period of $P = 346\text{d}$. This (unpublished) result appeared temporarily on the California Planet Search exoplanet website (as noted by Correia et al. (2008)) and was picked up on the Extrasolar Planets Encyclopedia (Schneider 2009). However, when it became apparent that a significant residual trend had skewed the Keplerian model, the link was removed from our website while additional data were collected. Although the initial fit was incorrect, one advantage of this early notice to

the community is that the star was added to the NACO direct imaging survey at the VLT (Chauvin et al. 2006) and a low mass stellar companion was imaged, HD 196885 B, with an angular separation of only $0''.7$ corresponding to a projected linear separation of 23 AU. Chauvin et al. (2007) report that photometry of the stellar companion is consistent with an M1V dwarf star with a mass of 0.5 - 0.6 M_{\odot} .

9.1. Stellar Characteristics

HD 196885 A (HIP101966) is a F8V star with absolute visual magnitude M_V of 3.79. The apparent stellar magnitude is $V=6.39$, and color is $B-V = 0.509$. The Hipparcos parallax is 0.0303 arcseconds, placing this star at a distance of 33 parsecs. We obtained a spectroscopic solution, iterating to obtain the same value for $\log g$ in the Y2 isochrones. We measure $T_{\text{eff}} = 6254 \pm 44\text{K}$, $\log g = 4.31 \pm 0.1$, $v \sin i = 7.8 \pm 0.50 \text{ km s}^{-1}$, and $[\text{Fe}/\text{H}] = 0.22 \pm 0.04 \text{ dex}$. Including a bolometric luminosity correction of -0.028, we obtain a stellar luminosity of 2.4 L_{\odot} from the Y2 stellar evolutionary tracks, with a radius of 1.31 R_{\odot} and mass of 1.28 M_{\odot} . The stellar age from evolutionary tracks is 3.12 (2.72, 3.48) Gyr (Takeda et al. 2007). Isaacson & Fischer (2009) measure $S_{\text{HK}} = 0.148$ and $\log R'_{\text{HK}} = -4.98$, indicating low chromospheric activity for HD 196885 A. Based on the activity level, we estimate a stellar rotation period of 9.4 days and intrinsic radial velocity jitter of 2 m s^{-1} . Stellar parameters for HD 196885 A are summarized in Table 1.

9.2. Doppler Observations and Keplerian Fit

As noted at the beginning of this section, HD 196885 A has an M dwarf stellar companion with a projected separation of only 23 AU. The time series velocities are plotted in Figure 10 and show an obvious large amplitude trend with curvature, caused by the stellar companion. The reflex velocities from the stellar orbit are modulated by a lower amplitude variation from a planet orbiting the primary component of this binary star system.

The observation dates, radial velocities, and uncertainties for HD 196885 A are listed in Table 8. Seventy-five observations have been obtained at Lick Observatory since 1998 July. Figure 10 shows the time series radial velocity measurements with a Keplerian model that is the combination of a planet model plus a stellar binary orbit. In fitting the Keplerian orbit, we added 2 m s^{-1} in quadrature to the internal errors as the best estimate for stellar noise based on the spectral type and activity of the star. However, we note that the close M dwarf companion will contaminate the spectrum of the primary star, increasing our Doppler

errors. We first tested periods from 30 to 100 years for the stellar companion detected by Chauvin et al. (2007). With a double-Keplerian model for the binary star and planet, we found that χ_ν^2 decreases to a minimum of 1.43 for orbital periods greater than about 40 years. However, χ_ν^2 is flat for longer orbital periods, out to ~ 200 years with strong covariances in the solutions in the orbital elements (K and the period) of the stellar binary system.

The best fit Keplerian solution for the planetary orbit, HD 196885 Ab, was determined with a Levenberg-Marquardt search of parameter space, which is reliable with phase coverage spanning several orbits. Our best fit model has an orbital period of 1333 ± 15 d, eccentricity 0.48 ± 0.06 , velocity semi-amplitude $K = 53.9 \pm 3.7$. The residuals to the fit of HD 196885 Ab have an RMS of 14.7 m s^{-1} and $\chi_\nu^2 = 1.58$. The Keplerian solution for the planet orbit is summarized in Table 3.

Figure 12 shows the modeled Keplerian orbit for HD 196885 Ab after the orbit from the assumed stellar binary HD 196885 B companion has been subtracted off. The contribution of light from the spatially unresolved M dwarf companion should be less than 1 part in 1000, but may have added systematic errors in our Doppler analysis that resulted in the poorer fit. Figure 12 shows the (stellar binary) residual velocities after the planetary orbit from HD 196885 Ab is removed. Clearly, the fractional phase of the observed stellar is not enough to constrain the period, amplitude or eccentricity of its orbit.

HD 196885 was also observed with ELODIE and CORALIE from June 1997 to August 2006. Correia et al. (2008) present those radial velocity data and include a longer time baseline of lower precision CORAVEL data to add modest constraints to the stellar binary orbit. They model acceptable periods ranging from 40 to 120 years for the stellar binary system. Their orbital solution for the planet, HD 196885 Ab, has a period of 3.69 years, eccentricity of 0.462, and velocity semi-amplitude of $40.5 \pm 2.3 \text{ m s}^{-1}$. We cannot resolve the inconsistency between their velocity amplitude and the larger velocity amplitude of $53.9 \pm 3.7 \text{ m s}^{-1}$ that we measure.

10. Discussion

We report Doppler velocities for six exoplanet discoveries from Lick Observatory. The planets are all more massive than Jupiter and have significant orbital eccentricity with periods ranging from 0.9 to 7.6 years. HD30562b has $M \sin i = 1.29 M_{\text{Jup}}$, an orbital eccentricity of 0.76, and an orbital period of 3 years. HD 86264b has $M \sin i = 7 M_{\text{Jup}}$, eccentricity of 0.7 and an orbital period of 4 years. HD 87883b has a mass, $M \sin i = 1.78 M_{\text{Jup}}$, eccentricity of 0.53 and an orbital period of 7.6 years. HD89307b has $M \sin i = 1.78 M_{\text{Jup}}$, eccentricity

of 0.241 and an orbital period of 5.9 years. HD148427b has a mass, $M \sin i = 0.96 M_{\text{Jup}}$, a more modest eccentricity of 0.16 and an orbital period of 0.9 years. HD196885Ab has $M \sin i = 2.58 M_{\text{Jup}}$, eccentricity of 0.48 and an orbital period of 3.65 years. Among the planets presented in this paper, the high mass planets orbit at wider separations and have higher eccentricity orbits.

The host stars HD 86264 and HD 148427 are essentially identical in mass ($M_* \approx 1.4 M_{\odot}$) and chemical composition ($[\text{Fe}/\text{H}] \approx +0.2$), but differ in their evolutionary states. HD 86264 is a F7V star, while HD 148427 resides on the subgiant branch as a K0IV star. Like most massive main-sequence stars, HD 86264 has moderate rotation with $v \sin i = 12.8 \text{ km s}^{-1}$ and modest chromospheric activity. As a result, the Doppler precision is much poorer for HD 86264 than for HD 148427 with internal errors of 19 m s^{-1} vs 6.8 m s^{-1} , respectively. Therefore, it would have been impossible to detect the planet found around HD 148427 if it had been orbiting a dwarf star of the same mass, like HD 86264. This emphasizes the value in searching for planets around stars in their cooler, evolved states (Johnson et al. 2007; Sato et al. 2008).

Before the detection of planets orbiting other stars, it was expected that exoplanets would reside on nearly circular orbits, like planets in our own solar system, as a result of eccentricity damping in protoplanetary disks. However, about one third of Doppler-detected exoplanets have measured orbital eccentricities greater than 0.3. As a result, a number of mechanisms have been proposed for exciting eccentricity in the orbits of gas giant planets (see Ford & Rasio (2008) and extensive references therein), including perturbations by stellar companions, scattering in the protoplanetary disk, resonant interactions between planet embryos and tidal interactions with the disk.

Planet-planet interactions appear to provide a mechanism that is able to reproduce the observed eccentricity distribution. After dissipation of the protoplanetary disk, eccentricities can grow rapidly and lead to gravitational encounters between planets (Chatterjee et al. 2008; Ford & Rasio 2008; Juric & Tremaine 2008). (Ford & Rasio 2008) find that simulations of encounters between unequal mass planets produce fewer collisions and a broader range of final eccentricities that reproduce the observed eccentricity distribution. Juric & Tremaine (2008) find that there are many different sets of initial conditions that can lead to similar “relaxed” eccentricity distributions and note that details of initial conditions may therefore be impossible to deduce from the final observed states. In order to explain the observed eccentricity distribution, Juric & Tremaine (2008) expect that one or two additional gas giant planets must reside in most exoplanet systems. A natural outcome of planet-planet scattering, a significant number of ejected planets and non-coplanar systems are expected.

HD196885A is a star with a massive planet in a binary stellar system. While exoplanets

have been found in several binary systems, this system is unusual because of the small projected linear separation of the stellar components. The current best solution places the M dwarf companion at a projected angular separation corresponding to only 23 AU. One of the challenges for planet formation models is the growth of planetesimals from meter-sized objects to kilometer-sized objects. This challenge is even greater in close binary systems, yet the primary star hosts a fairly massive planet with a semi-major axis of 2.37 AU. A good measurement of the semi-major axis of the stellar binary would help to understand how this planet could have formed and survived the dynamics of this challenging environment.

Most of the host stars presented in this paper have high (super-solar) metallicity. Thus, we note that the planet-metallicity correlation for gas giant planets (Fischer & Valenti 2005; Santos, Israelian & Mayor 2004) continues to hold for longer orbital periods.

We gratefully acknowledge the dedication and support of the Lick Observatory staff. DAF acknowledges research support from NASA grant NNX08AF42G. JAJ is an NSF Astronomy and Astrophysics Postdoctoral Fellow with support from the NSF grant AST-0702821. A.W.H gratefully acknowledges support from a Townes Postdoctoral Fellowship at the U.C. Berkeley Space Sciences Laboratory. The authors extend thanks to those of Hawaiian ancestry on whose sacred mountain of Mauna Kea we are privileged to be guests. Without their kind hospitality, the Keck observations of HD 87883 would not have been possible. This research has made use of the SIMBAD database, operated at CDS, Strasbourg, France, and of NASA’s Astrophysics Data System Bibliographic Services.

REFERENCES

- Baliunas, S. L., et al. 1995, ApJ, 438, 269
- Baliunas, S. L., Henry, G. W., Donahue, R. A., Fekel, F. C. & Soon, W. H. 1997, ApJ, 474, L119
- Bouchy, F., Mayor, M., Lovis, C., Udry, S., Benz, W., Bertaux, J.-L., Delfosse, X., Mordasini, C., Pepe, F., Queloz, D. & Segransan, D., A&A, 496, 572
- Butler, R. P., Marcy, G. W., Williams, E., McCarthy, C., Dosanjh, P. & Vogt, S. S. 1996, PASP, 108, 500
- Butler, R. P., Wright, J. T., Marcy, G. W., Fischer, D. A., Vogt, S. S., Tinney, C. G., Jones, H. R. A., Carter, B.D., Johnson, J. A., McCarthy, C., Penny, A. J. 2006, ApJ, 646, 505
- Chatterjee, S., Ford, E. B., Matsumura, S., Rasio, F. A. 2008, ApJ, 686, 580
- Chauvin, G., Lagrange, A.-M., Udry, S., Fusco, T., Galland, F., Naef, D., Beuzit, J.-L. & Mayor, M. 2006, A&A, 456, 1165
- Chauvin, G., Lagrange, A.-M., Udry, S. & Mayor, M. 2007, A&A, 475, 723
- Correia, A. C. M., et al. 2008, A&A, 479, 271
- Demarque, P., Woo., J.-H., Kim, Y.-C. & Yi, S. K. 2004, ApJS, 155, 667
- Duncan, D. K., et al. 1991, ApJS, 76, 383
- Driscoll, P., Fischer, D. & Ford, E. 2009, ApJ, in press
- ESA 1997, The Hipparcos and Tycho Catalogs. ESA-SP 1200
- Fischer, D. A. & Valenti, J. A. 2005, ApJ 622, 1102
- Fischer, D. A., Marcy, G.W., Butler, R. P., Vogt, S.S. & Apps, K. 1999, PASP111, 50
- Ford, E. B. 2005, AJ, 129, 1706
- Ford, E. B., Rasio & Rasio, F. A. 2008, ApJ, 686, 621
- Giguere, M. & Fischer, D.A. 2009, ApJ(in prep)
- Henry, G. W. 1999, PASP, 111, 845

- Henry, G. W., Fekel, F. C., & Henry, S. M. 2007, *AJ*, 133, 1421
- Howard, A. W., Johnson, J. A., Marcy, G. W., Fischer, D. A., Wright, J. T., Henry, G. W., Giguere, M. J., Isaacson, H., Valenti, J. A., Anderson, J. & Piskunov, N. E. 2009, *ApJin* press
- Isaacson, H. & Fischer, D.A. 2009, *ApJ* in prep
- Johnson, J. A., Fischer, D. A., Marcy, G. W., Wright, J. T., Driscoll, P., Butler, R. P., Hekker, S., Reffert, S., Vogt, S. S. 2007, *ApJ*, 665, 785
- Jurić, M., Tremaine, S. 2008, *ApJ*, 686, 603
- Marcy, G. W. & Butler, R. P. 1992, *PASP*, 104, 270
- Marcy, G. W., Butler, R. P., Williams, E., Bildsten, L., Graham, J. R., Ghez, A. M. & Jernigan, J. G. 1997, *ApJ*, 481, 926
- Marcy, G., Butler, R. P., Fischer, D., Laughlin, G., Vogt, S., Henry, G. & Pourbaix, D. 2002, *ApJ*, 581, 1375
- Mayor, M., Bonfils, X., Forveille, T., Delfosse, X., Udry, S., Bertaux, J. -L., Beust, H., Bouchy, F., Lovis, C., Pepe, F., Perrier, C., Queloz, D., Santos, N. C. 2009, *arXiv0906.2780*
- Mayor, M., Udry, S., Lovis, C., Pepe, F., Queloz, D., Benz, W., Bertaux, J.-L., Bouchy, F., Mordasini, C., Segransan, D. 2009, *Å*, 493, 639
- Moutou, C., Mayor, M., Lo Curto, G., Udry, S., Bouchy, F., Benz, W., Lovic, C., Naef, D., Pepe, F., Queloz, D. & Santos, N.-C. 2009, *A&A*, 496, 513
- Noyes, R. W., Hartmann, L., Baliunas, S. L., Duncan, D. K. & Vaughan, A. H. 1984, *ApJ*, 279, 763
- Queloz, D., Henry, G. W., Sivan, J. P., Baliunas, S. L., Beuzit, J. L., Donahue, R. A., Mayor, M., Naef, D., Perrier, C. & Udry, S. 2001, *A&A*, 379, 279
- Saar, S. H., Butler, R. P. & Marcy, G. W. 1998, *ApJ*, 498, 153
- Saar, S. H. & Fischer, D. A. 2000, *ApJ*, 534, 105
- Santos, N. C., Israelian, G., Mayor, M. 2004, *A&A*, 415, 1153

- Sato, B., Izumiura, H., Toyota, E., Kambe, E., Ikoma, M., Omiya, M., Masuda, S., Takeda, Y., Murata, D., Itoh, Y., Ando, H., Yoshida, M., Kokubo, E., & Ida, S. 2008, PASJ, 60, 539
- Schneider, J. 2009, <http://exoplanet.eu/catalog.php>
- Takeda, G., Ford, E. B., Sills, A., Rasio, F. A., Fischer, D. A., & Valenti, J. A. 2007, ApJS, 168, 297
- Valenti, J. A., Fischer, D. A., Marcy, G. W., Johnson, J. A., Henry, G. W., Wright, J. T., Howard, A. W., Giguere, M. & Isaacson, H. 2009, ApJ, in press
- Valenti, J. A. & Fischer, D. A. 2005, ApJS, 159, 141
- Valenti, J. A. & Piskunov, N. 1996, A&A, 118, 595
- Vogt, S. S. et al. 1994, SPIE, 2198, 362.
- Vogt, S. S. 1987, PASP, 99, 1214
- VandenBerg, D. A. & Clem, J. L. 2003, AJ, 126, 778
- Wright, J. T. 2005, PASP, 117, 657
- Wright, J. T. & Howard, A. 2009, ApJ(in press)

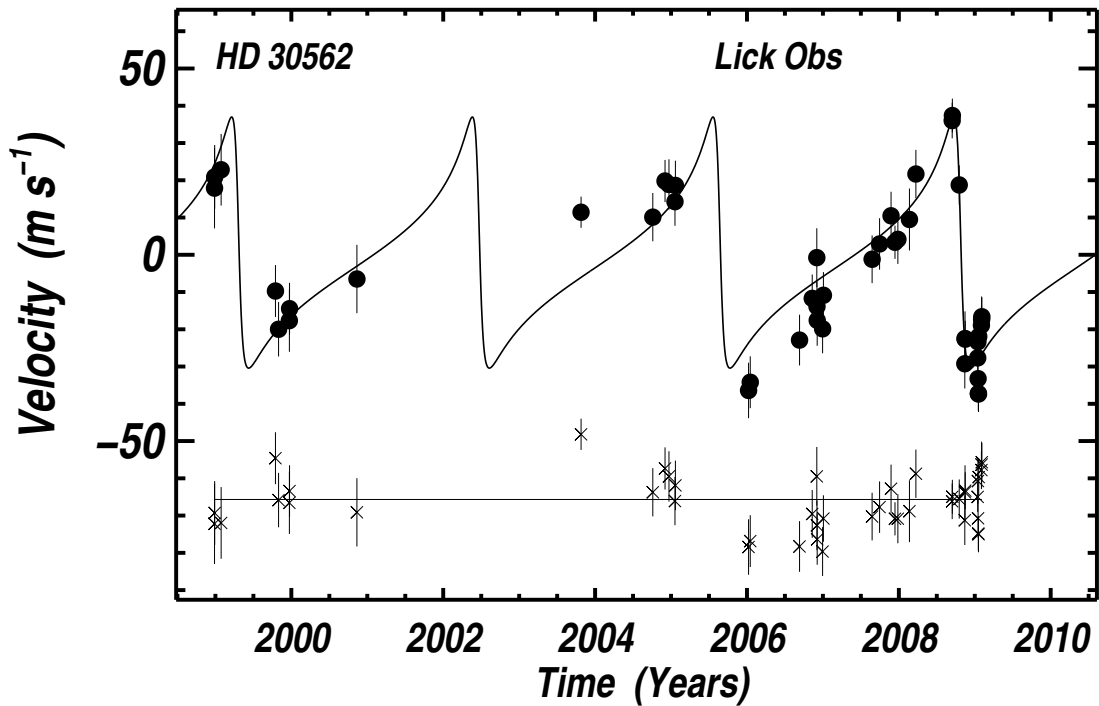


Fig. 1.— Time series radial velocities from Lick Observatory are plotted for HD 30562 with 2.9 m s^{-1} of expected velocity jitter added in quadrature with the single measurement uncertainties. The Keplerian model is overplotted with an orbital period of 3.2 years, velocity amplitude of 33.7 m s^{-1} and eccentricity, $e = 0.76$. With these parameters and the stellar mass of $1.219 M_{\odot}$, we derive a planet mass, $M \sin i = 1.29 M_{\text{Jup}}$ and semi-major axis of 2.3 AU. Residual velocities to the fit are offset and show some slight systematic variation.

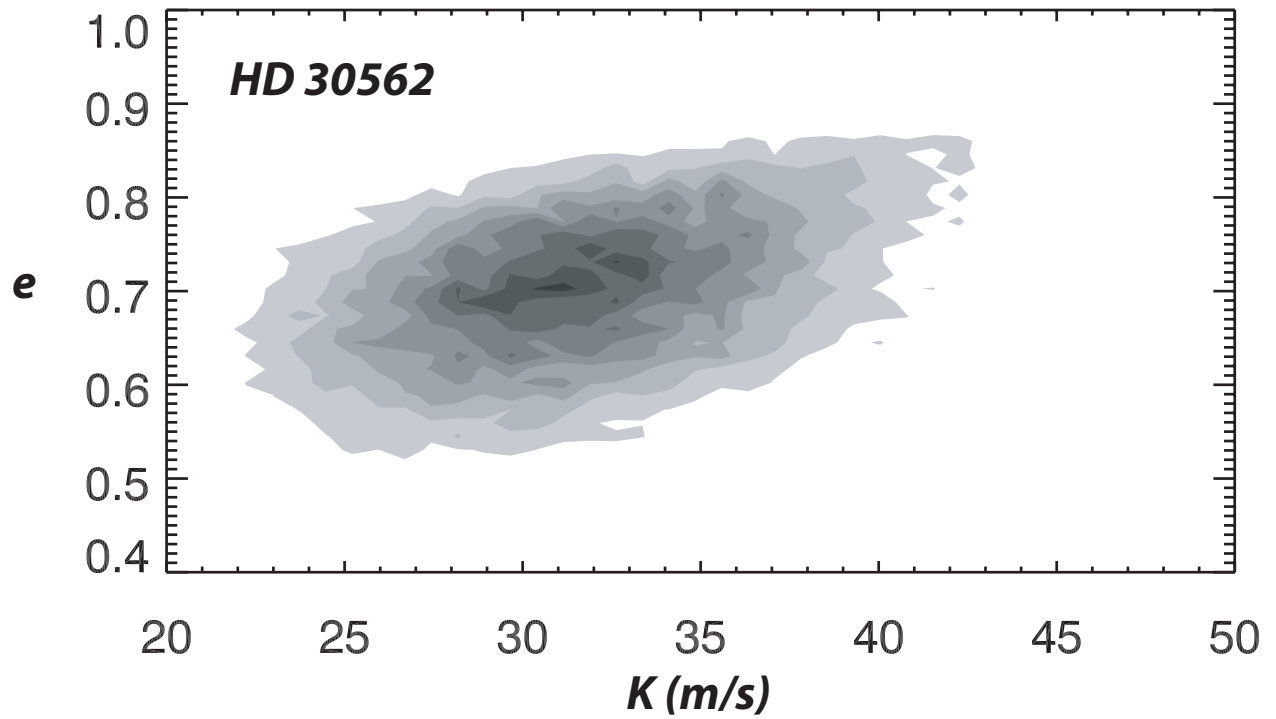


Fig. 2.— The MCMC analysis reveals a modest covariance between the orbital eccentricity and velocity amplitude that is a factor of two larger than the formal errors from the LMMC analysis.

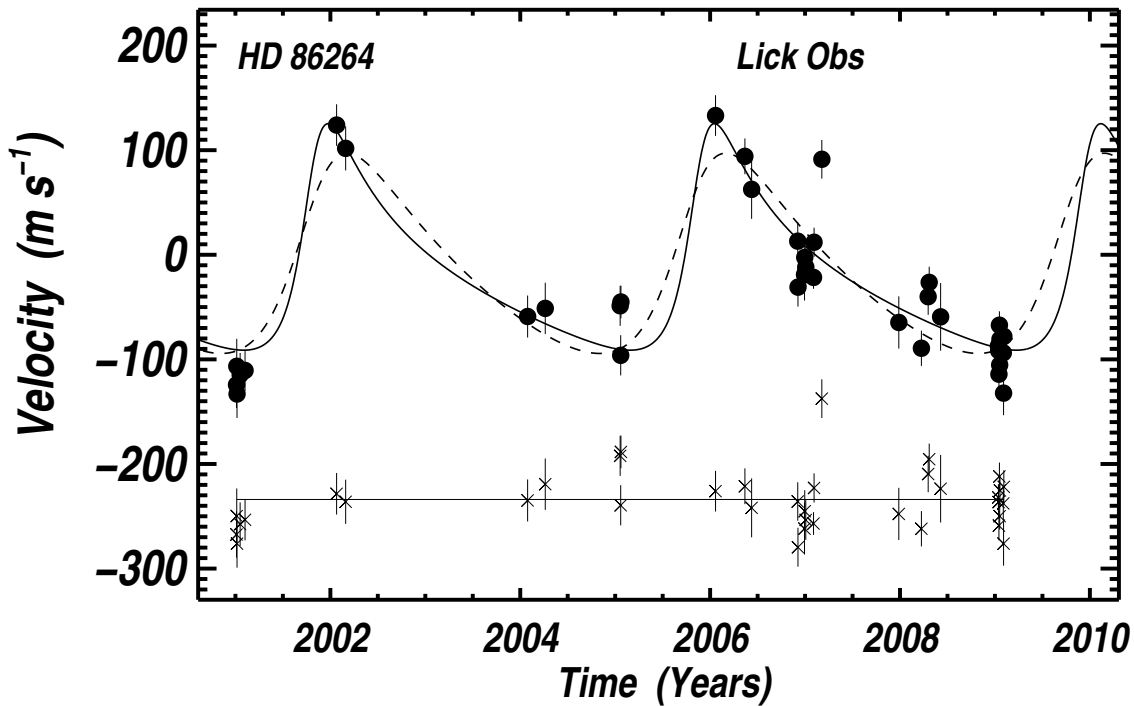


Fig. 3.— Time series radial velocities for HD 86264 from Lick Observatory. The best fit Keplerian orbit is plotted as a solid line and has an orbital period of almost 4 years, a velocity amplitude of 132 m s^{-1} and eccentricity of 0.7. The stellar mass of $1.42 M_{\odot}$ yields a planet mass, $M \sin i = 7 M_{\text{Jup}}$ and semi-major axis of 2.86 AU. An alternative Keplerian model with an eccentricity of 0.4 is shown with a dashed line. Such a model has a χ^2_{ν} fit that is only worse by 5% compared to the 0.7 eccentricity solution.

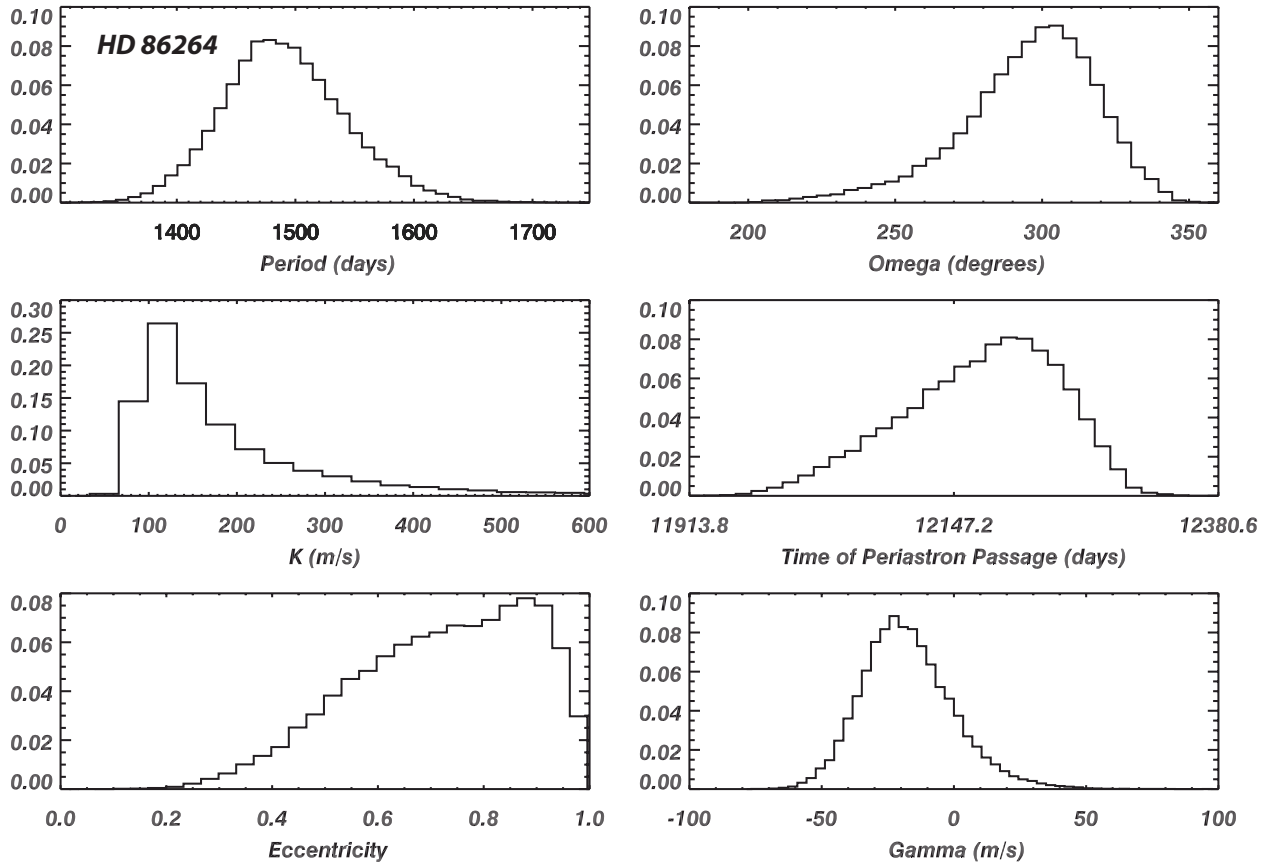


Fig. 4.— The posterior probability distributions from Markov Chain Monte Carlo (MCMC) simulations show peak values close to those derived from Levenberg-Marquardt fitting. The widths of these distributions characterize the uncertainty in the orbital parameters.

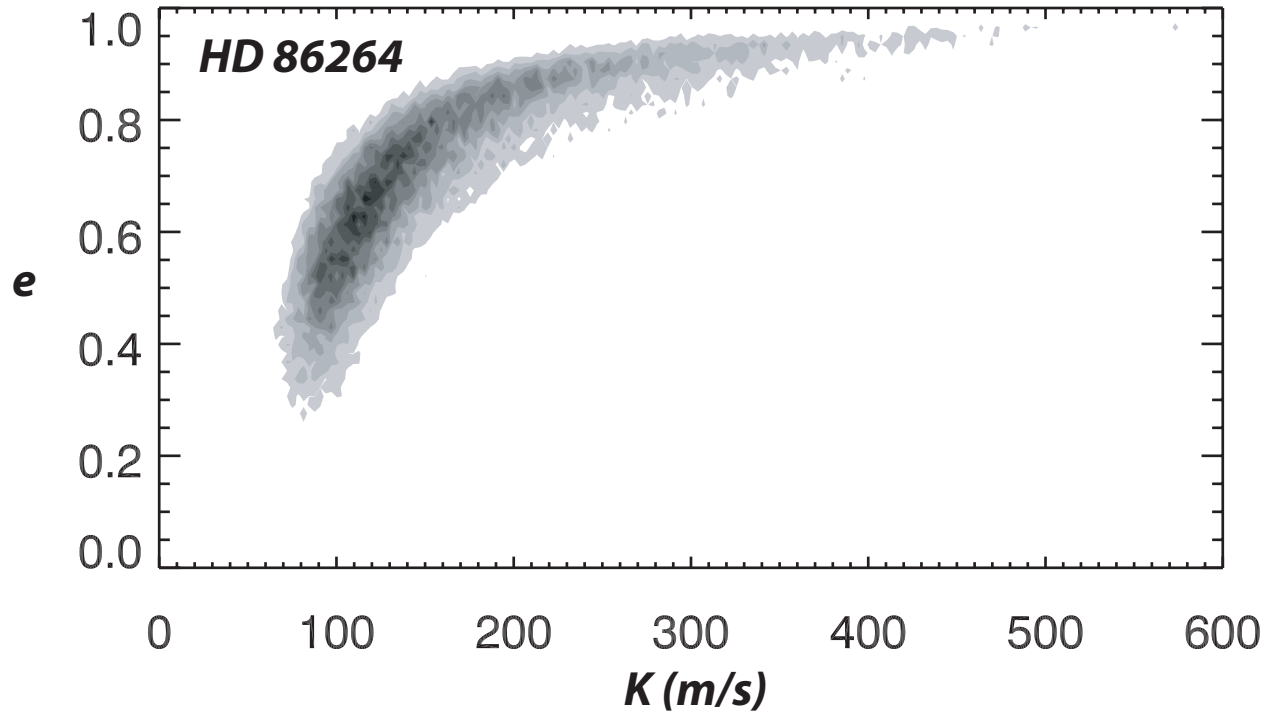


Fig. 5.— The MCMC probability density functions used to model the Keplerian orbital parameters reveals covariance between orbital eccentricity and velocity amplitude. For the most likely velocity amplitude of about 132 m s^{-1} , eccentricities between 0.5 and 0.7 are plausible.

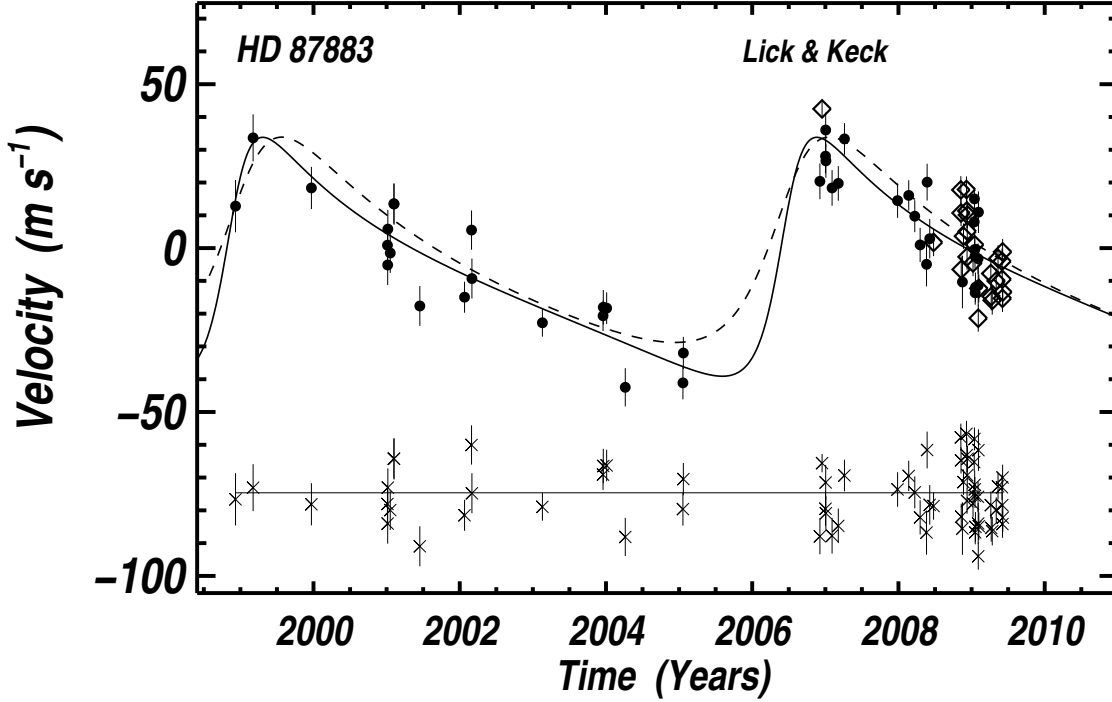


Fig. 6.— Our time series Doppler measurements from Lick Observatory are shown with filled circles and velocities from the Keck Observatory are represented by diamonds. We have added 4.5 m s^{-1} velocity jitter in quadrature to both of the error bars shown here. The best fit Keplerian orbital period is 7.6 years, the eccentricity for this planet is $e = 0.53$ and the velocity semi-amplitude is $K = 34.7 \text{ m s}^{-1}$. Because there is a gap in the phase approaching periastron, the eccentricity is poorly constrained and values as low as 0.4 are plausible for this star. With the stellar mass of $0.82 M_{\odot}$ we derive a planet mass, $M \sin i = 1.78 M_{\text{Jup}}$ and semi-major axis of 3.6 AU. The best fit theoretical curve is overplotted with a solid line and the lower eccentricity solution is plotted with a dashed line.

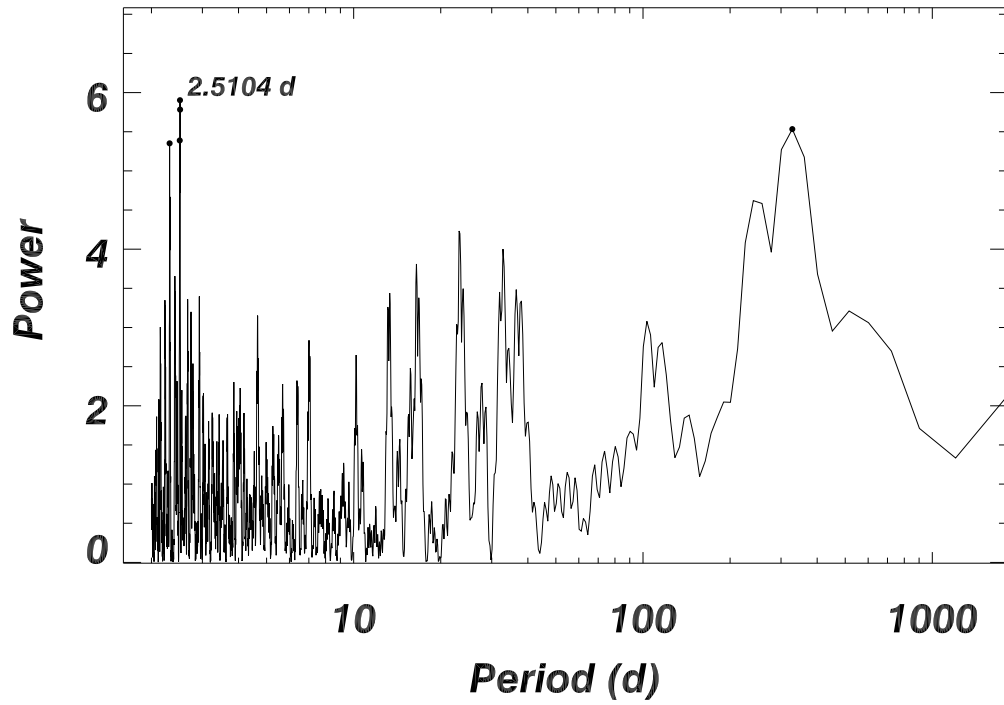


Fig. 7.— Periodogram of residuals to the Keplerian model of HD 87883 for higher cadence, higher precision Keck radial velocities. A modest peak appears at 2.5 days, but we do not consider this to be significant. The residual Keck data do not show any period with an FAP below 5%.

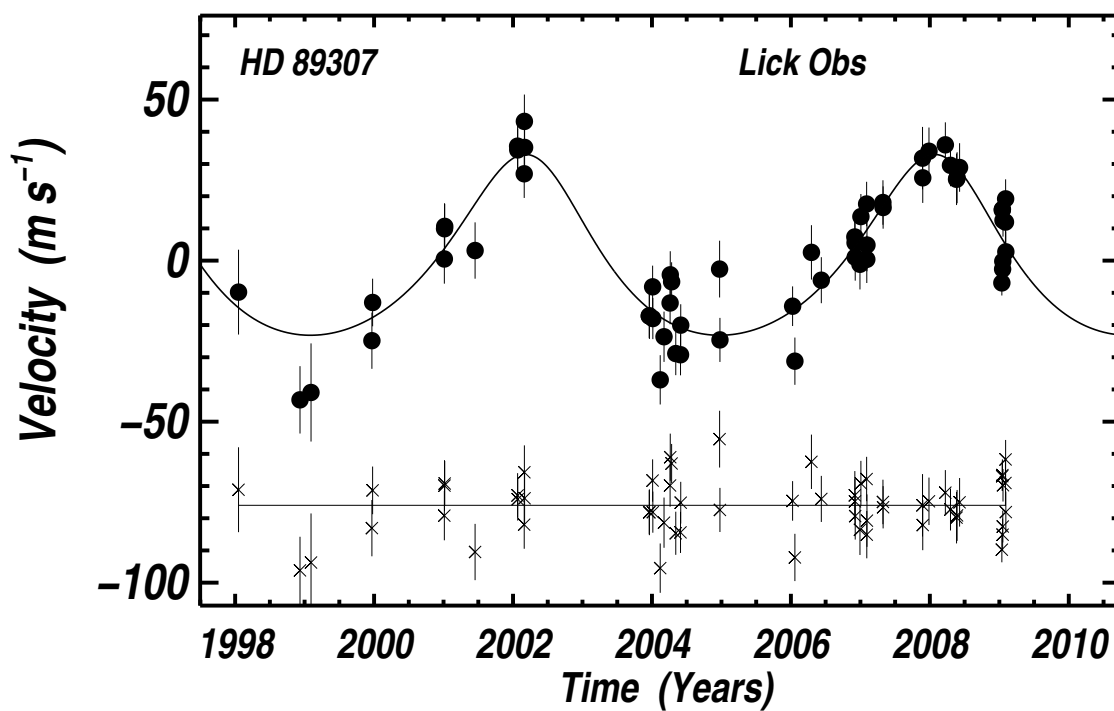


Fig. 8.— Radial velocities from Lick Observatory are plotted for HD 89307, including 2.8 m s^{-1} of jitter added in quadrature to the internal errors. The best fit Keplerian model is overplotted with a solid line and yields an orbital period 5.9 years, velocity amplitude of 28.9 m s^{-1} and eccentricity of 0.24. With the assumed stellar mass of $1.028 M_{\odot}$ we derive a planet mass, $M \sin i = 1.78 M_{\text{Jup}}$ and semi-major axis of 3.27 AU.

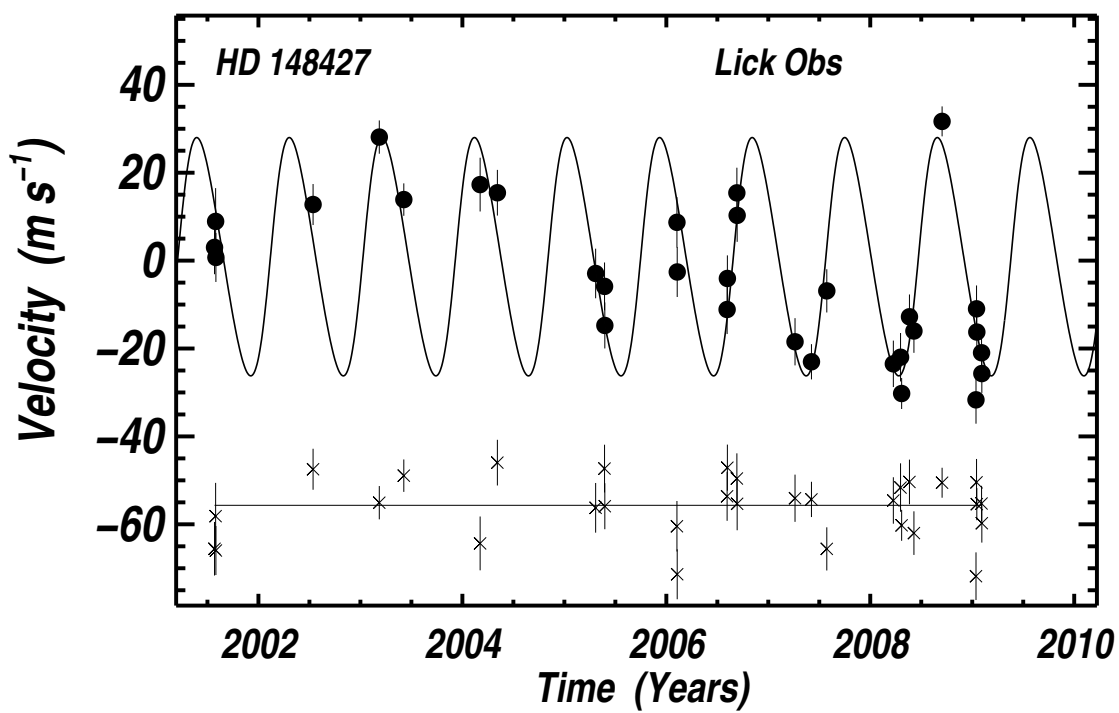


Fig. 9.— Time series radial velocities are shown for the K0IV star, HD 148427 and include 3.5 m s^{-1} of jitter added in quadrature with the formal measurement errors. The dashed line shows a Keplerian best fit model with an orbital period of 0.9 years, velocity amplitude of 27.7 m s^{-1} and eccentricity of 0.16. Adopting a stellar mass of $1.45 M_{\odot}$ we derive a planet mass, $M \sin i = 0.96 M_{\text{Jup}}$ and orbital radius of 0.93 AU.

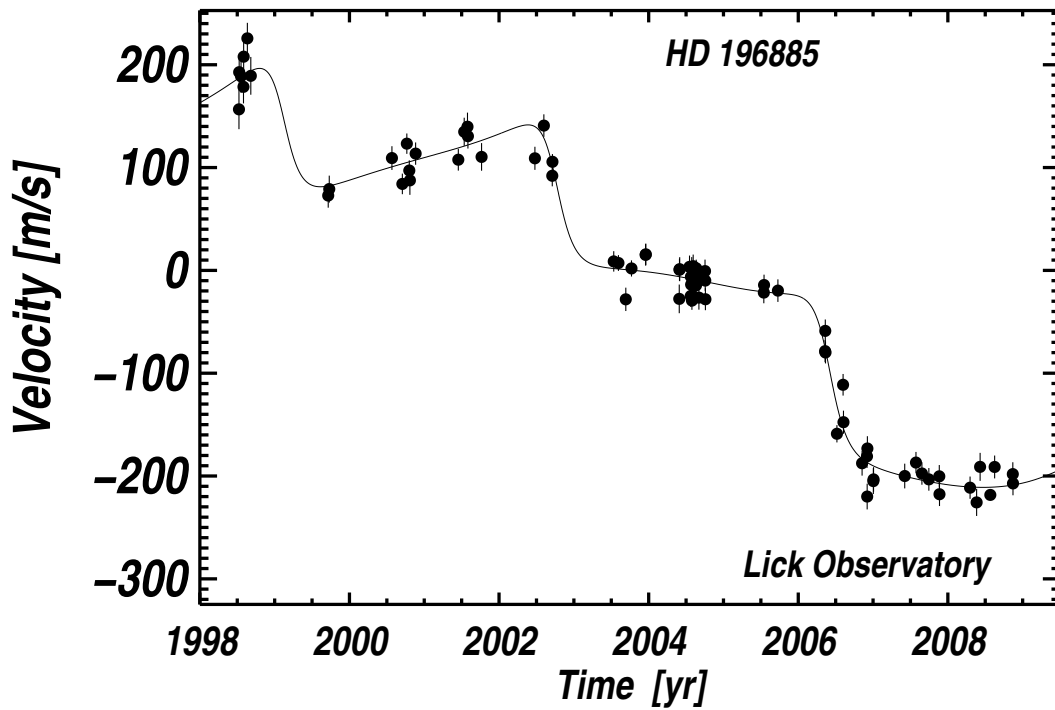


Fig. 10.— Time series radial velocities for HD 196885 are best fit with a double Keplerian model that includes the known M dwarf stellar companion and a second planetary companion. An assumed jitter of 2 m s^{-1} was added in quadrature to the formal uncertainties to model this system.

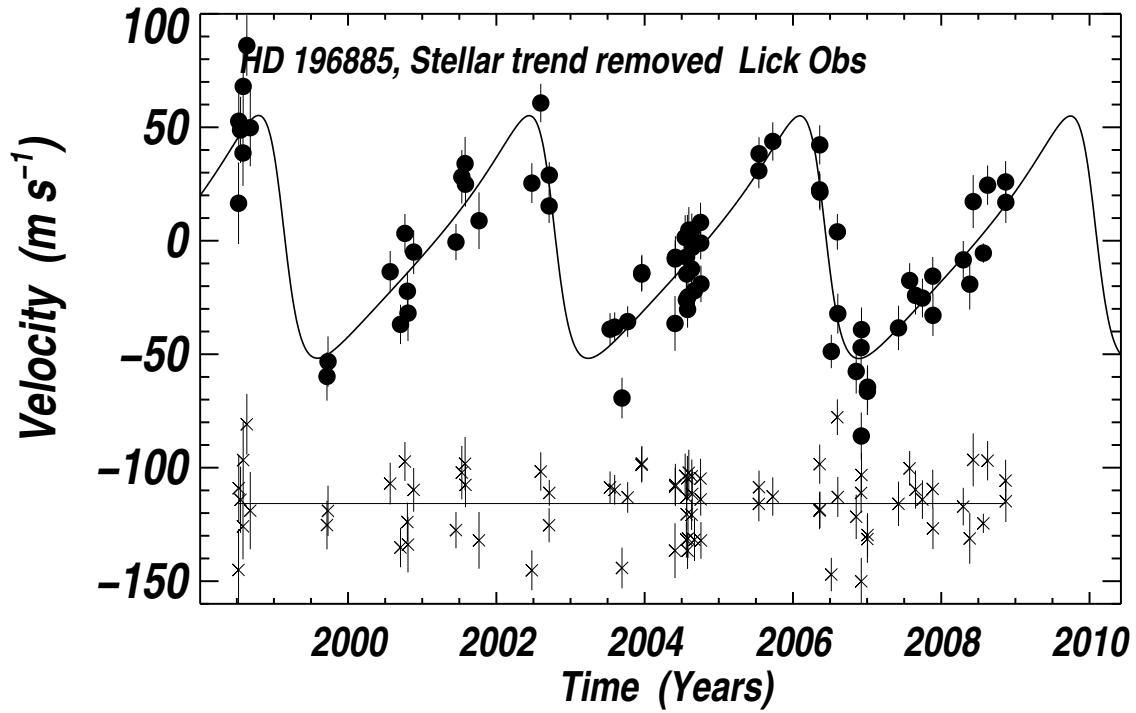


Fig. 11.— The Keplerian model for HD 196885Ab is shown with the Keplerian model for the stellar companion subtracted off. The residual data are best fit by a planetary companion with $M \sin i = 2.58 M_{\text{Jup}}$ in an orbit with a semi-major axis of 2.37 AU.

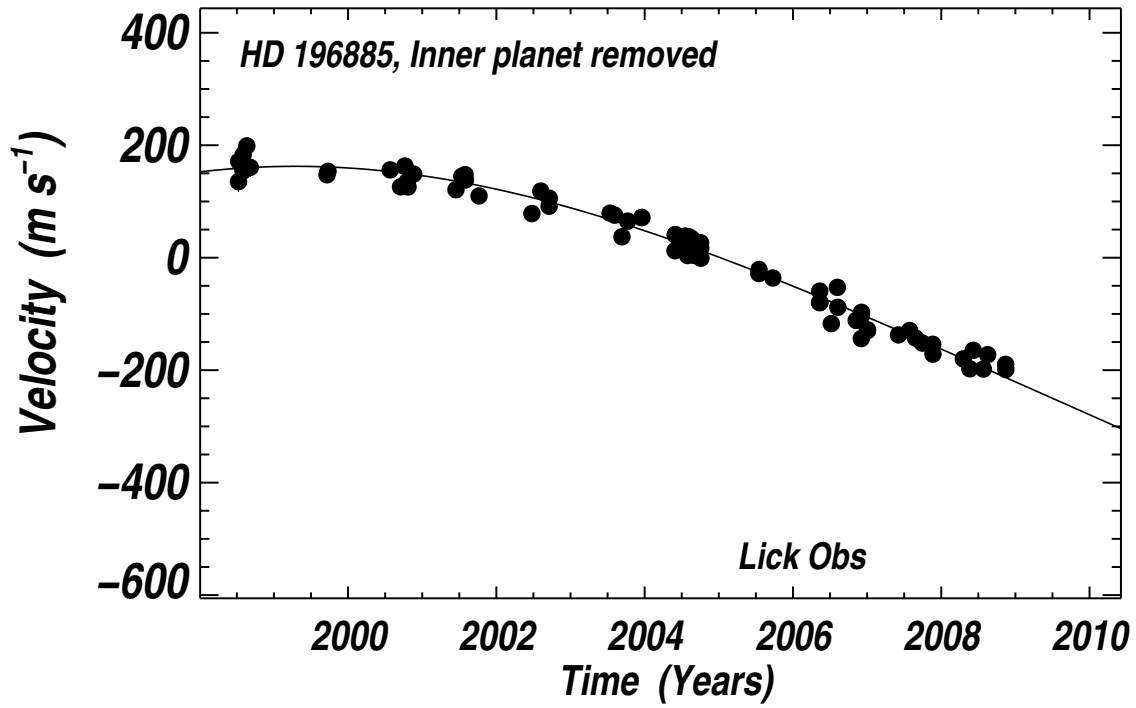


Fig. 12.— Residual velocities for HD 196885 A are plotted after removing the modeled velocities from the planet. The Keplerian model for the stellar companion has a fixed period of 120 years, however the phase coverage is poor and the χ^2_{ν} fit is nearly constant for periods from 40 to 200 years.

Table 1. Stellar Parameters

Parameter	HD 30562	HD 86264	HD 87883	HD 89307	HD 148427	HD 196885A
Spectral Type	F8V	F7V	K0V	G0V	K0IV	F8V
Distance (pc)	26.5	72.6	18.1	30.9	59.3	33
$B - V$	0.63	0.46	0.96	0.640	0.93	0.509
T_{eff} (K)	5861 (44)	6210 (44)	4980 (44)	5950 (44)	5052 (44)	6254 (44)
$\log g$	4.09 (0.10)	4.02 (0.10)	4.58 (0.10)	4.414 (0.10)	3.59 (0.10)	4.31 (0.10)
[Fe/H]	+0.243 (0.04)	+0.202 (0.04)	+0.093 (0.04)	-0.14 (0.04)	+0.154 (0.04)	+0.22 (0.04)
$v \sin i \text{ km s}^{-1}$	4.9 (0.50)	12.8 (0.50)	2.17 (0.50)	3.21 (0.50)	2.13 (0.5)	7.8 (0.50)
V	5.77	7.42	7.57	7.06	6.89	6.39
BC	-0.064	-0.024	-0.305	-0.075	-0.26	-0.028
M_V	3.65	3.10	6.27	4.57	3.02	3.79
$L_{\star} (L_{\odot})$	2.85 (0.19)	4.55 (0.6)	0.318 (0.018)	1.24 (0.09)	6.09 (0.75)	2.41 (0.16)
$M_{\star} (M_{\odot})$	1.219 (0.04)	1.42 (0.05)	0.82 (0.04)	1.028 (0.04)	1.45 (0.06)	1.28 (0.05)
$R_{\star} (R_{\odot})$	1.637 (0.06)	1.88 (0.12)	0.76 (0.03)	1.05 (0.04)	3.22 (0.2)	1.31 (0.05)
S_{HK}	0.15 (0.005)	0.20 (0.017)	0.278 (0.021)	0.154 (0.008)	0.139 (0.017)	0.148 (0.018)
$\log R'_{\text{HK}}$	-5.064	-4.73	-4.81	-4.98	-5.18	-5.02
P_{rot} (d)	24.2	4.15	38.6	23.7	55.7	9.81
Age (Gyr)	4.0	2.24	9.8	6.76	2.5	3.12

Table 2. Radial Velocities for HD30562

JD-2440000	RV (m s ⁻¹)	σ_{RV} (m s ⁻¹)
11174.91602	17.82	10.03
11175.80664	20.83	7.57
11206.75391	22.75	8.74
11467.97958	-9.75	6.37
11482.93596	-20.05	6.73
11534.86523	-17.74	7.35
11535.85769	-14.54	5.67
11859.89453	-6.57	8.25
12937.90033	11.27	3.48
13282.98926	10.04	5.10
13341.85063	19.69	4.90
13360.80337	18.80	5.44
13389.76837	14.19	5.10
13391.77977	18.54	5.32
13743.72993	-36.48	6.28
13751.78702	-34.28	5.69
13988.95190	-22.96	5.50
14049.94301	-11.77	5.02
14071.95702	-0.83	6.80
14072.80531	-13.94	5.34
14073.86159	-17.66	5.54
14099.84141	-19.94	5.19
14103.77660	-10.93	4.77
14337.98200	-1.27	4.99
14374.02309	2.84	5.64
14428.95087	10.40	5.07
14447.83085	3.26	3.81
14461.87088	4.07	5.23
14517.65772	9.41	7.29

Table 2—Continued

JD-2440000	RV (m s ⁻¹)	σ_{RV} (m s ⁻¹)
14548.65551	21.61	5.11
14723.02289	35.82	3.85
14724.01284	37.37	3.55
14756.94272	18.69	4.43
14783.85702	-29.31	5.30
14784.89422	-22.55	6.08
14785.94216	-22.72	4.06
14845.77865	-27.85	3.24
14846.75067	-23.42	4.61
14847.73611	-32.97	4.38
14848.75761	-37.29	3.70
14849.72956	-37.37	3.92
14850.75859	-21.96	4.11
14863.74239	-18.96	4.57
14864.68794	-17.42	5.47
14865.70517	-16.68	4.62

Table 3. Orbital Parameters

Parameter	HD 30562b	HD 86264b	HD 87883b	HD 89307b	HD 148427b	HD 196885Ab
P (d)	1157 (27)	1475 (55)	2754 (87)	2157 (63)	331.5 (3.0)	1333 (15)
K (m s ⁻¹)	33.7 (2.2)	132 (33)	34.7 (4.5)	28.9 (2.2)	27.7 (2)	53.9 (3.7)
e	0.76 (0.05)	0.7 (0.2)	0.53 (0.12)	0.241 (0.07)	0.16 (0.08)	0.48 (0.06)
T_p (JD)	10131.5 (14)	15172 (114)	11139 (90)	10228 (80)	13991 (15)	11992 (12)
ω (deg)	81 (10)	306 (10)	291 (15)	36 (52)	277 (68)	78 (7.6)
Trend (m s ⁻¹ yr ⁻¹)	...	0.005
a (AU)	2.3 (0.02)	2.86 (0.07)	3.6 (0.08)	3.27 (0.07)	0.93 (0.01)	2.37 (0.02)
$M \sin i (M_{\text{Jup}})$	1.29 (0.08)	7.0 (1.6)	1.78 (0.34)	1.78 (0.13)	0.96 (0.1)	2.58 (0.16)
N_{obs}	45	37	69	59	31	76
jitter m s ⁻¹	2.9	3.3	4.5	2.8	3.5	2.0
RMS (m s ⁻¹)	7.58	26.2	9.2	9.9	7.0	14.7
χ^2_ν	1.31	1.21	1.71	1.37	1.08	1.58
FAP	< 0.0001	< 0.0001	< 0.0001	< 0.0001	< 0.0001	< 0.0001

Table 4. Radial Velocities for HD86264

JD-2440000	RV (m s ⁻¹)	σ_{RV} (m s ⁻¹)
11913.97949	-124.29	21.75
11914.95215	-106.63	25.94
11915.97266	-133.09	22.51
11927.95800	-114.71	20.32
11946.87109	-110.60	19.18
12298.95410	124.05	19.34
12333.84668	101.74	20.59
13033.93945	-58.99	19.57
13101.71289	-51.24	24.08
13389.83370	-48.75	18.64
13391.97233	-96.12	18.67
13392.81923	-45.12	14.91
13756.87898	133.09	19.13
13869.71119	94.29	16.79
13895.69225	62.54	27.79
14073.04851	13.04	17.77
14074.02220	-30.92	18.04
14099.03887	-18.92	24.35
14099.99183	-2.54	19.56
14103.92013	-11.77	18.46
14133.86964	-21.51	10.55
14135.79582	11.93	13.57
14165.79559	91.33	17.90
14461.93014	-64.70	24.53
14548.77584	-89.39	16.58
14574.75097	-40.01	16.78
14578.76834	-26.36	14.60
14622.69367	-59.33	31.96
14844.97356	-87.15	12.52

Table 4—Continued

JD-2440000	RV (m s ⁻¹)	σ_{RV} (m s ⁻¹)
14846.05428	-91.75	15.39
14846.97546	-114.10	13.59
14848.92699	-67.28	12.89
14849.87817	-105.34	12.34
14850.92234	-80.79	13.45
14863.88580	-93.69	16.25
14864.89708	-132.25	20.60
14865.90181	-78.03	15.50

Table 5. Radial Velocities for HD87883

JD-2440000	RV (m s ⁻¹)	σ_{RV} (m s ⁻¹)	Observatory
1998.93369	12.80	7.97	L
1999.17408	33.63	7.17	L
1999.97128	18.35	6.44	L
2001.01165	0.88	5.85	L
2001.01429	-5.14	6.10	L
2001.01709	5.80	5.87	L
2001.04992	-1.50	6.07	L
2001.09908	13.53	6.08	L
2001.10167	13.45	6.32	L
2001.45430	-17.65	6.10	L
2002.06567	-14.97	4.72	L
2002.16120	5.50	5.98	L
2002.16649	-9.29	6.11	L
2003.13049	-22.78	4.23	L
2003.96032	-20.66	4.64	L
2003.96316	-18.05	5.25	L
2004.00956	-18.31	4.81	L
2004.26352	-42.47	5.83	L
2005.05229	-41.12	5.03	L
2005.05815	-32.01	4.92	L
2006.92539	20.38	5.46	L
2006.95556	42.47	2.80	K
2007.00210	28.05	5.22	L
2007.00472	36.03	5.33	L
2007.00740	26.61	5.16	L
2007.09195	18.36	5.43	L
2007.17675	19.74	5.27	L
2007.26151	33.31	4.83	L
2007.98755	14.49	5.27	L

Table 5—Continued

JD-2440000	RV (m s ⁻¹)	σ_{RV} (m s ⁻¹)	Observatory
2008.14057	16.07	4.63	L
2008.22279	9.73	4.87	L
2008.29645	0.97	5.21	L
2008.38397	-4.94	6.73	L
2008.39214	20.11	5.62	L
2008.42769	2.86	6.03	L
2008.47985	1.75	4.16	K
2008.85326	17.75	4.20	K
2008.85584	10.71	4.01	K
2008.85868	-6.52	3.96	K
2008.87491	-10.34	8.02	L
2008.88886	3.65	3.88	K
2008.92978	17.89	3.96	K
2008.93511	11.34	5.32	K
2008.93805	-2.68	3.92	K
2008.94051	5.14	4.05	K
2008.94338	10.12	3.93	K
2009.02007	-4.52	4.02	K
2009.03607	7.99	2.81	L
2009.03925	15.00	3.49	L
2009.04198	1.03	4.21	K
2009.04426	-0.41	3.77	L
2009.04697	-2.47	3.67	L
2009.04970	-13.64	3.63	L
2009.05243	-11.98	4.53	L
2009.08818	-3.23	4.63	L
2009.09078	-11.39	6.23	L
2009.09116	-21.38	4.11	K
2009.09359	10.95	6.34	L

Table 5—Continued

JD-2440000	RV (m s ⁻¹)	σ_{RV} (m s ⁻¹)	Observatory
2009.09890	-12.31	4.24	K
2009.26318	-7.77	4.14	K
2009.26863	-14.77	4.20	K
2009.28229	-15.93	4.35	K
2009.33710	-10.03	3.82	K
2009.36175	-3.13	3.99	K
2009.41635	-4.02	3.86	K
2009.41906	-9.49	3.92	K
2009.42181	-15.32	4.16	K
2009.42461	-1.15	3.94	K
2009.42729	-13.37	4.31	K

Table 6. Radial Velocities for HD89307

JD-2440000	RV (m s ⁻¹)	σ_{RV} (m s ⁻¹)
10831.87988	-9.78	12.67
11155.06152	-43.23	9.82
11212.96387	-40.94	14.81
11533.03711	-24.86	7.96
11536.94238	-13.00	6.46
11914.03613	0.51	6.77
11914.97949	9.90	7.03
11916.00391	10.64	6.00
12075.69141	3.13	7.97
12299.01562	35.54	5.90
12299.81152	34.38	5.56
12333.89355	26.96	6.57
12334.78516	43.23	7.53
12335.84668	35.15	7.04
12991.03027	-17.15	5.84
12992.05762	-17.21	6.13
13009.01367	-8.14	5.50
13009.97070	-17.99	5.28
13048.88880	-37.26	7.21
13068.85645	-23.63	6.92
13100.75994	-13.11	6.25
13101.78418	-4.40	6.38
13108.80719	-6.78	5.50
13130.74121	-28.86	5.65
13155.68164	-29.22	5.29
13156.69141	-20.03	5.39
13361.03331	-2.62	8.45
13362.97417	-24.75	6.35
13744.96252	-14.16	4.98

Table 6—Continued

JD-2440000	RV (m s ⁻¹)	σ_{RV} (m s ⁻¹)
13756.89883	-31.22	6.39
13843.85424	2.56	7.64
13895.70819	-6.08	6.18
14072.05486	7.35	6.63
14073.05723	5.55	5.96
14074.03192	1.07	6.34
14099.05421	-1.15	6.93
14103.99258	13.67	6.01
14133.92363	17.59	5.87
14134.86984	0.39	6.40
14135.81388	4.83	7.31
14219.75881	18.05	5.90
14220.77130	16.48	5.49
14428.07576	31.82	9.01
14429.07464	25.71	6.91
14461.97798	33.97	6.42
14547.88772	35.95	5.99
14574.81520	29.59	5.42
14606.73102	25.25	7.14
14609.71447	25.74	7.05
14622.73115	28.91	6.63
14844.94877	-6.94	3.47
14846.99865	15.72	3.79
14847.99892	15.93	4.15
14848.94512	-2.65	4.31
14849.93880	-0.10	4.24
14850.94371	12.47	4.37
14863.93069	12.09	6.65
14864.88307	19.22	5.49

Table 6—Continued

JD-2440000	RV (m s ⁻¹)	σ_{RV} (m s ⁻¹)
14865.91973	2.72	5.84

Table 7. Radial Velocities for HD148427

JD-2440000	RV (m s ⁻¹)	σ_{RV} (m s ⁻¹)
12117.77468	3.02	5.84
12121.73047	8.93	7.15
12122.74609	0.73	4.99
12470.75977	12.77	3.94
12707.99301	28.24	3.50
12795.82135	13.79	3.39
13069.05859	17.30	5.59
13130.97559	15.45	4.56
13482.91224	-2.92	5.06
13514.81401	-5.86	4.83
13515.77733	-14.75	4.61
13774.07313	8.72	5.17
13775.06466	-2.58	5.11
13953.67145	-11.12	4.99
13954.67293	-4.05	4.61
13988.64826	15.42	5.15
13989.64802	10.30	5.48
14196.94310	-18.46	4.76
14255.88785	-23.03	3.60
14310.74223	-6.88	4.23
14549.03808	-23.48	4.66
14574.91787	-21.97	4.91
14578.89804	-30.23	3.05
14606.89543	-12.78	4.42
14622.86542	-16.01	4.29
14723.66497	31.67	2.92
14845.09173	-31.67	5.13
14847.10053	-10.97	4.69
14848.09531	-16.06	3.20

Table 7—Continued

JD-2440000	RV (m s ⁻¹)	σ_{RV} (m s ⁻¹)
14865.07943	-20.97	3.61
14866.07445	-25.72	4.03

Table 8. Radial Velocities for HD196885A

JD -2440000.	RV (m s ⁻¹)	Uncertainties (m s ⁻¹)
11004.87786	156.62	17.99
11005.91113	192.76	14.54
11014.87598	188.81	14.59
11026.84668	178.52	14.52
11027.87109	207.85	16.91
11045.85156	225.65	13.38
11062.77637	189.21	17.01
11440.64692	72.65	10.70
11445.72070	79.05	11.09
11751.85840	109.24	9.18
11802.79239	84.09	8.69
11824.63919	123.29	8.56
11836.69527	97.32	8.54
11839.62402	87.54	12.24
11867.63857	113.28	9.64
12075.96484	107.64	7.97
12104.88281	134.78	11.78
12120.84375	139.73	11.79
12122.85938	130.53	9.83
12189.63457	110.52	12.50
12449.96387	109.00	8.79
12493.81152	140.81	8.45
12534.77637	92.01	7.53
12535.67998	105.53	5.70
12834.92419	8.73	7.03
12857.93443	7.09	6.51
12893.79688	-28.15	8.96
12921.69336	2.33	6.73
12990.64258	15.11	7.78

Table 8—Continued

JD -2440000.	RV (m s ⁻¹)	Uncertainties (m s ⁻¹)
12991.59863	15.60	7.85
13154.95898	-27.71	12.08
13155.92090	0.59	8.15
13156.95117	1.17	9.31
13204.88432	3.41	9.82
13210.93750	-24.94	7.91
13211.91406	-6.21	7.52
13212.85449	-13.81	6.89
13215.90261	1.96	9.82
13216.86158	-30.02	8.00
13218.85502	-24.73	8.53
13222.87458	4.10	10.15
13236.80479	-14.96	6.69
13237.80842	2.00	7.35
13239.87256	-5.86	10.66
13250.83496	-26.50	9.40
13280.76758	-0.69	8.72
13281.72754	-9.92	7.17
13282.69531	-28.07	8.07
13567.90576	-21.60	7.69
13568.94066	-14.24	7.28
13636.69163	-19.68	8.45
13866.95528	-78.52	8.18
13867.88733	-58.85	8.63
13868.98856	-79.86	8.03
13924.88196	-159.16	7.36
13954.79810	-111.27	7.85
13956.86757	-147.65	8.80
14047.64309	-187.58	9.78

Table 8—Continued

JD -2440000.	RV (m s ⁻¹)	Uncertainties (m s ⁻¹)
14071.60554	-180.85	8.84
14072.60604	-219.97	10.38
14073.57926	-173.23	9.71
14102.59081	-204.95	10.44
14103.58541	-203.28	9.64
14255.98494	-199.99	9.78
14310.86948	-186.92	7.63
14339.83862	-197.52	8.41
14373.72263	-203.25	8.51
14424.65135	-200.30	8.46
14425.58582	-217.71	9.11
14575.00470	-211.34	8.28
14606.98432	-225.65	11.16
14623.95213	-191.09	11.68
14673.88099	-219.00	4.25
14694.90059	-191.19	8.66
14783.63365	-198.13	9.19
14784.60365	-207.20	9.13